Korean J. Chem. Eng., 40(10), 2538-2554 (2023)
DOI: 10.1007/s11814-023-1438-7

pISSN: 0256-1115
eISSN: 1975-7220

Effect of thermal radiation and magnetic field on heat transfer of SWCNT/water nanofluid inside a partially heated hexagonal cavity

Milad Alizadeh*, Amin Fazlollahtabar*, Ahmed Kadhim Hussein, Hussein Ali Ameen***, D. D. Ganji*, Uddhaba Biswal****,†, and Bagh Ali*****

*Mechanical Engineering Department, Babol Noshirvani University of Technology, Babol, Iran
**College of Engineering - Mechanical Engineering Department, University of Babylon, Babylon City, Iraq
***Department of Computer Techniques Engineering, Al-Mustaqbal University College, Hillah 51001, Iraq
****Department of Mathematics, Laxminarayan College, Jharsuguda, 768201, Odisha, India
*****School of Mechanical Engineering and Automation, Harbin Institute of Technology, Shenzhen, 518055, China
(*Received 19 September 2022 • Revised 29 January 2023 • Accepted 3 February 2023*)

Abstract−The interaction between the magneto-hydrodynamic buoyant convection and the radiation in a partly heated hexagonal enclosed space filled with SWCNTs/water nanoliquid was inspected in the current work for the first time. The lowermost wall of the enclosed space was partially heated, while the other regions of this wall were presumed thermally insulated. The upper wall was considered insulated also. The four inclined walls of the enclosed space were maintained at a constant cold temperature. A magnetic field with magnitude, B_o is enforced on the enclosed space. The enclosed space was included inside it a concave hexagonal shaped body under three different conditions at its boundary namely (cold, adiabatic and heated). The outcomes of the present work are obtained for diverse Hartmann number, Rayleigh number varied as $10^4 \le Ra \le 10^6$, heated region length varied as $0.1 \le L_T \le 0.4$, various conditions of the internal hexagonal body (cold, adiabatic and heated), solid volume fraction diverse as $0 \le \phi \le 0.04$ and radiation parameter varied as $0 \le R_d \le 1$. In the present work, the standard Galerkin finite element method (SGFEM) is employed to model the fluid flow and heat transfer. It is established that the Nusselt number along the heated bottom wall of the hexagonal enclosed space (Nu_{out}) rises as Rayleigh number rises. The same increasing is seen for the velocity distribution along vertically mean position. The stream function and Nu_{out} decrease as the Hartmann number increases. The stream function, temperature and velocity have the maximum profiles at the heated condition followed by the adiabatic one, while the cold condition has the minimum profile.

Keywords: Nanoliquid, Free Convection, Magnetic Field, Hexagonal Cavity, Radiation

INTRODUCTION

Natural convection in an enclosed enclosure is considered as one of most interesting problems in the scientific society. This increased attention goes back to the wide applications of this phenomenon in engineering and technology [1-3]. Some of these applications include thermal storage systems, condensers, refrigerators, cooling of electronic components, nuclear reactors, heating and cooling systems of buildings and solar collectors [4-8]. From another side, the interaction between the Lorentz force coming from the magnetic field and the buoyancy force or the so-called magneto-hydrodynamic (MHD) natural convection or magneto-convection has a significant importance in various technological applications like crystal growth in liquids, fire researches, plasma studies, microelectronic devices, fusion reactors, electromagnetic launch technology, metal casting, geothermal energy extraction and nuclear engineering [9-12].

From another aspect, most of the classical heat transfer liquids, such as water, ethylene-glycol, and mineral oil, have a low heat transfer efficiency due to their low thermal conductivity. This problem can be resolved by adding solid nanoparticles with a high thermal conductivity to these fluids. The resulting fluid coming from the combination of the classical fluid and solid nanoparticles is called a nanofluid [13,14]. This efficient and smart fluid has attracted enormous attention among scientists and engineers, since it can be deliberated as a heat valve to control the temperature flow. Also, it can be applicable in numerous industrial applications, such as solar stills and collectors, compact heat exchangers, cooling of computer processors, pool boiling, air-conditioning and cooling applications, oil industry and automobile radiators [15-17]. For further details about the nanofluid and its applications one can be return to many good papers like Esfe et al. [18], Bazdar et al. [19], Arasteh et al. [20], Ruhani et al. [21] and Kamel et al. [22]. It is beneficial to mention that the natural convection in a hexagonal enclosed space can be considered as an attractive subject due to its complex heat transfer mechanism [23]. Kumar et al. [24] explored numerically the interaction of the convection and surface radiation in a hexagonal enclosed space. They deduced that surface radiation had an important effect on buoyant convection and increased the strength of the flow circulation inside the enclosed space.

Nowadays, the natural convection phenomenon inside complex shaped cavities filled with a nanofluid has a widespread applications

†To whom correspondence should be addressed.
E-mail: uddhababiswal789@gmail.com

in technology and industry, such as solar collectors, air-conditioning, thermal design of buildings, and cooling of electronic circuit boards [25-29]. The problem of the MHD convection in these boxes filled with a nanoliquid has been investigated by many researchers. The MHD free convection in an L-shaped cavity filled with water-Al_2O_3 nanoliquid was carried out by Sourtiji and Hosseinizadeh [30]. They gathered that the heat transfer rate was increased by reducing the Hartmann number and increasing the solid volume fraction. Sheikholeslami et al. [31] presented a numerical analysis of the magneto-hydro-convection in a semi-annulus cavity. The outcomes showed that the heat energy transfer rate was a declining function of Ra and an increasing function of Ha. The outcome of the magnetic field on the buoyant convection in a slanted L-shape cavity filled with Al_2O_3 - water nanoliquid was explored numerically by Sheikholeslami et al. [32]. It was found that the Nusselt number was enhanced by increasing the solid volume fraction and Ra. Whereas, it was reduced by increasing the inclination angle and Ha. The numerical exploration of the free convection in a semi-circular shape enclosed space was done by Al-Zamily [33]. This space was filled with a copper-water nanoliquid and subjected to a localized thermal source at its bottom wall. A vertical magnetic field was applied to the enclosed space. The mean Nusselt number was decreased by decreasing the solid volume fraction and Ra. While, it was increased by decreasing Ha. El-Shehabey et al. [34] worked on MHD regular convection in a slanted L-shaped cavity filled with water-copper nanoliquid. The mathematical simulation of MHD free convection in a slanted T-shaped cavity was carried out by Hussein et al. [35]. The influences of the particle-volume fraction, aspect ratio, (Ra) and (Ha) numbers, tilting angle and length and place of the heat source on the flow and thermal fields were investigated. Four different nanoparticles were used inside the cavity: TiO_2, Al_2O_3, Ag, Cu; while the water was taken as a base liquid. They deduced that the averaged Nusselt number was reduced by decreasing the particle volume fraction, heat source location, and the tilting angle. Ali et al. [36] explored mathematically MHD convection in a hexagonal enclosed space with a tilted square block. This space was filled with water-CuO nanofluid. Both the tilted walls of the block and horizontal barriers of the enclosed space were preserved at a constant hot temperature. Yadollahi et al. [37] calculated numerically the buoyant convection in an "F-shaped" box filled with Ag-water nanoliquid. The box was subjected to a horizontal magnetic field from its left vertical hot wall. It was noted that the averaged Nusselt number was decreased by increasing the Hartmann number, whereas it reached its peak value at AR=0.4. A numerical investigation of the magneto-hydrodynamic natural convection in a complex-shape enclosure filled with CuO-water nanoliquid was carried out by Dogonchi et al. [38]. It was found that the enhancement in the local and mean Nusselt numbers reached their maximum value for low Hartmann number and higher Rayleigh number. The impact of the magnetic field on the buoyant convection in a tilted V-shaped chamber filled with water-copper nanofluid was numerically carried out by Purusothaman and Malekshah [39]. Their analysis was done for module aspect ratio varying as $0.2 \le AR \le 0.8$, Hartmann number varying as $0 \le Ha \le 80$), solid volume fraction varying as $0\% \le \phi \le 6\%$, Rayleigh number varying as $10^4 \le Ra \le 10^6$ and inclination angle varying as $0^o \le \gamma \le 225^o$. They demonstrated that the mean Nusselt number was raised by increasing Ra and reducing Ar and Ha. Recently, Seyyedi et al. [40] explored the magnetic field influence on the free convection and the entropy generation in a wavy-hexagonal porous box filled with water-copper nanofluid. The results showed that when the solid volume fraction increased, the average Nusselt number was increased, while the entropy generation number was decreased. For further references about the natural convection in a complex shaped chambers filled with a nanoliquid, the reader can find them in [41-46].

On the other hand, the combined effect of thermal radiation and convection in enclosures has significant attention due to its major importance in many advanced industrial fields. Samples of these fields cover material drying, transpiration cooling process and advanced energy convection system functioning at high temperature [47,48]. The combined effects of free convection and radiation in a semi annulus filled with Fe_3O_4-water nanoliquid was studied numerically by Sheikholeslami et al. [49]. The enclosed space was exposed to a non-uniform magnetic field. The results are presented for wide values of Ha, magnetic number, particle-volume fraction and Rayleigh number. They gathered that the mean Nusselt number was amplified by rising the magnetic number, solid volume fraction and R and decreasing the radiation parameter and Ha. Recently, Li et al. [50] did numerical work on MHD convection and entropy generation in a tilted square cavity filled with water-Al_2O_3 nanoliquid. The cavity had included inside it a circular hot baffle and the effect of the radiation was taken. It was found that both the radiation and the nanoliquid enhanced entropy production and heat energy transfer rate in the cavity.

However, in light of the above literature survey, the magneto-hydrodynamic buoyant convection and its interaction with the radiation in a partly heated hexagonal enclosed space filled with SWCNTs/water nanoliquid was never measured previously in any article before this work. So, the present work is an original attempt to investigate and analyze both the flow and thermal fields in this unique geometry. Moreover, the number of the published papers related to a hexagonal cavity is very limited compared with another geometries of cavities.

GEOMETRICAL CONFIGURATION AND THE GOVERNING EQUATIONS

Figs. 1 and 2 illustrate, respectively, a schematic drawing and the mesh spreading of the two-dimensional hexagonal enclosed space. The enclosed space was filled with SWCNTs/water nanoliquid. The bottom barrier of it was partially heated, while the regions of this wall were presumed adiabatic. The top barrier was considered adiabatic also. The four inclined barriers of the enclosed space were retained at a constant cold temperature (T_c). The enclosed space had included inside it a concave hexagonal shaped body under three different conditions at its boundary: cold, adiabatic and heated. A magnetic field with uniform magnitude, B_o, was imposed on the enclosed space. The gravitational force was presumed to act in the opposite y-direction. The impact of thermal radiation and natural convection was considered. The thermo-physical properties are specified in Table 1. The governing PDEs are simplified by using the subsequent assumptions:

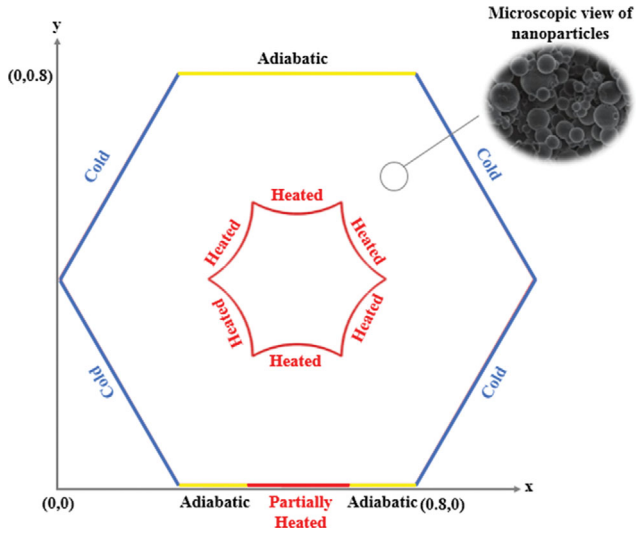

Fig. 1. Schematic diagram.

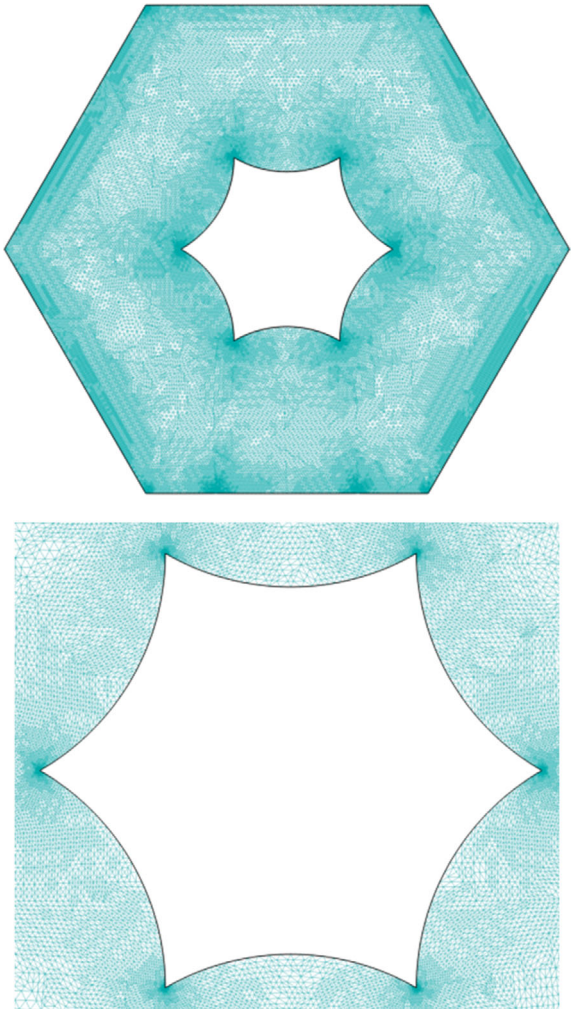

Fig. 2. Mesh of the computational domain.

- The thermo-physical properties are presumed as constant except for the density difference due to Boussinesq model.

Table 1. Thermophysical values of nanoparticle & water

Property	Water	SWCNT
$\rho\left(\frac{kg}{m^3}\right)$	997.1	2,600
$k\left(\frac{W}{mK}\right)$	0.613	6,600
$C_p\left(\frac{J}{kgK}\right)$	4,179	425
$\beta\left(\frac{1}{K}\right)$	21×10^{-5}	$33\times10^{-}7$

- The nanoparticles have a uniform shape and size and are finely mixed with the base liquid.
- Water and nanoparticles are in thermal equilibrium state and no slip occurs between them.
- The stream is considered laminar, Newtonian, and steady.

Considering the above assumptions, the governing equations of the problem are [42]:

$$\frac{\partial u}{\partial x}+\frac{\partial v}{\partial y}=0 \tag{1}$$

$$\rho_{nf}\left(u\frac{\partial u}{\partial x}+v\frac{\partial u}{\partial y}\right)=-\frac{\partial p}{\partial x}+\mu_{nf}\left(\frac{\partial^2 u}{\partial x^2}+\frac{\partial^2 u}{\partial y^2}\right), \tag{2}$$

$$\rho_{nf}\left(u\frac{\partial v}{\partial x}+v\frac{\partial v}{\partial y}\right)=-\frac{\partial p}{\partial y}+\mu_{nf}\left(\frac{\partial^2 v}{\partial x^2}+\frac{\partial^2 v}{\partial y^2}\right)$$
$$-\frac{\sigma}{\rho_{nf}}B_0^2 v-g\rho_{nf}\beta_{nf}(T^*-T_C), \tag{3}$$

$$u\frac{\partial T^*}{\partial x}+v\frac{\partial T^*}{\partial y}=\alpha_{nf}\left(\frac{\partial^2 T^*}{\partial x^2}+\frac{\partial^2 T^*}{\partial y^2}\right)-\left(\frac{1}{(\rho C_p)_{nf}}\right)\frac{\partial q_r}{\partial y},$$
$$\text{where, } q_r=-\left(4\frac{\sigma_r}{\chi_r}\right)\frac{\partial T^4}{\partial y},\ T^4\cong-3T_C^4+4T_C^3T \tag{4}$$

In these equations, u and v denote the velocity components in the x and y directions. T^* shows the temperature and p stands for the pressure. Moreover, the thermophysical properties of the nanofluid, including the density, viscosity, coefficient of thermal expansion and thermal diffusivity, are presented as ρ_{nf}, μ_{nf}, β_{nf} and α_{nf}, respectively. Moreover, the following boundary conditions are considered for the problem:

Along the outer walls

At the inclined side walls:

$$T^*=T_C \tag{5}$$

At bottom:

$$\begin{cases}\frac{\partial T^*}{\partial y}=0, \text{ Adiabatic parts}\\ T^*=T_h, \text{ Partially heated part}\end{cases} \tag{6}$$

At top:

$$\frac{\partial T^*}{\partial y}=0 \tag{7}$$

At all walls:

$$u=v=0 \tag{8}$$

Along the inner walls:

At all inner concave hexagonal shaped walls:

$$T^{*}=T_h \tag{9}$$

Moreover, the thermophysical properties of the nanoliquid are calculated as [42]:

$$\begin{cases} \beta_{nf}=(1-\phi)\beta_f+\phi\beta_p, \\ \rho_{nf}=(1-\phi)\rho_f+\phi\rho_p, \\ (\rho C_p)_{nf}=(1-\phi)(\rho C_p)_f+\phi(\rho C_p)_p, \\ \alpha_{nf}=\dfrac{k_{nf}}{(\rho C_p)_{nf}}, \\ \dfrac{k_{nf}}{k_f}=\dfrac{(1-\phi)+2\phi\left(\dfrac{k_p}{k_p-k_f}\right)\ln\left(\dfrac{k_p-k_f}{2k_f}\right)}{(1-\phi)+2\phi\left(\dfrac{k_f}{k_p-k_f}\right)\ln\left(\dfrac{k_p+k_f}{2k_f}\right)}, \\ \dfrac{\mu_{nf}}{\mu_f}=\dfrac{1}{(1-\phi)^{2.5}}, \end{cases} \tag{10}$$

where β_f, β_p, ρ_f, ρ_p, $(C_p)_f$, $(C_p)_p$, k_f and k_p are the thermal expansion coefficient, density, specific heat capacity and thermal conductivity of the base fluid and nanoparticles, respectively. Moreover, μ_f denotes the dynamic viscosity of the base fluid and ϕ stands for the nanoparticles volume fraction.

Following non-dimensional variables are considered in the governing equations:

$$X=\frac{x}{L},\ Y=\frac{y}{L},\ U=\frac{uL}{\alpha_f},\ V=\frac{vL}{\alpha_f},\ T=\frac{T^{*}-T_C}{T_h-T_C},\ P=\frac{pL^2}{\rho_f\alpha_f^2},\ \vartheta_f=\frac{\mu_f}{\rho_f},$$

$$Pr=\frac{\vartheta_f}{\alpha_f},\ Ra=\frac{\beta_f(T_h-T_C)L^3}{\vartheta_f\alpha_f},\ Ha=B_0L\sqrt{\frac{\sigma}{\rho_{nf}\vartheta_f}},\ Rd=\frac{4\sigma_r T_C^3}{\chi_r k_f},$$

$$P=-\gamma\left(\frac{\partial U}{\partial X}+\frac{\partial V}{\partial Y}\right).$$

Here, Ra, Pr, Ha and Rd represent the Rayleigh number, Prandtl number, Hartmann number and radiation parameter. Also, the value of γ is equal to 10^7, which is used for eliminating the pressure from these equations. By using these variables, the non-dimensional form of PDEs are as follows [42]:

$$\frac{\partial U}{\partial X}+\frac{\partial V}{\partial Y}=0 \tag{12}$$

$$U\frac{\partial U}{\partial X}+V\frac{\partial U}{\partial Y}=\gamma\frac{\rho_f}{\rho_{nf}}\frac{\partial}{\partial X}\left(\frac{\partial U}{\partial X}+\frac{\partial V}{\partial Y}\right)+Pr\frac{\vartheta_{nf}}{\vartheta_f}\left(\frac{\partial^2 U}{\partial X^2}+\frac{\partial^2 U}{\partial Y^2}\right), \tag{13}$$

$$U\frac{\partial V}{\partial X}+V\frac{\partial V}{\partial Y}=\gamma\frac{\rho_f}{\rho_{nf}}\frac{\partial}{\partial Y}\left(\frac{\partial U}{\partial X}+\frac{\partial V}{\partial Y}\right)+Pr\frac{\vartheta_{nf}}{\vartheta_f}\left(\frac{\partial^2 V}{\partial X^2}+\frac{\partial^2 V}{\partial Y^2}\right)$$
$$-Ha^2PrV+\frac{(1-\phi)\rho_f\beta_f+\phi\rho_p\beta_p}{\rho_{nf}\beta_{nf}}RaPrT, \tag{14}$$

$$U\frac{\partial T}{\partial X}+V\frac{\partial T}{\partial Y}=\frac{\alpha_{nf}}{\alpha_f}\left(\frac{\partial^2 T}{\partial X^2}+\frac{\partial^2 T}{\partial Y^2}\right)+\frac{4}{3}Rd\frac{(\rho C_p)_f}{(\rho C_p)_{nf}}\frac{\partial^2 T}{\partial Y^2}, \tag{15}$$

Also, the boundary conditions in the non-dimensional form are:

At the inclined side walls:

$$T=0 \tag{16}$$

At bottom:

$$\begin{cases} \dfrac{\partial T}{\partial Y}=0, \text{ Adiabatic parts} \\ T=1, \text{ Partially heated part} \end{cases} \tag{17}$$

At top:

$$\frac{\partial T}{\partial Y}=0 \tag{18}$$

At all walls:

$$U=V=0 \tag{19}$$

At all inner concave hexagonal shaped walls:

$$T=1 \tag{20}$$

The average Nusselt number for the partly heated domain of enclosed space is defined as:

$$Nu_{ave}=\int_{L_T}\left(1+\frac{4}{3}\frac{k_f}{k_{nf}}Rd\right)\left(\frac{k_{nf}}{k_f}\right)\frac{\partial T}{\partial n}dX, \tag{21}$$

where, n is the normal direction at the hot wall of the enclosed space (L_T).

NUMERICAL TECHNIQUE AND VALIDATION

In the present work, the standard Galerkin finite element method (SGFEM) is employed to model the fluid flow and heat transfer. The phase-change procedure is solved by cubic interpolation over the triangles [51,52]. The calculation of problems dealing with the triangle grids is accomplished on the nodes. In this technique, the equations are formed by replacing the descriptions, applying the dependencies to the variables, integrating over cells, and differenti-

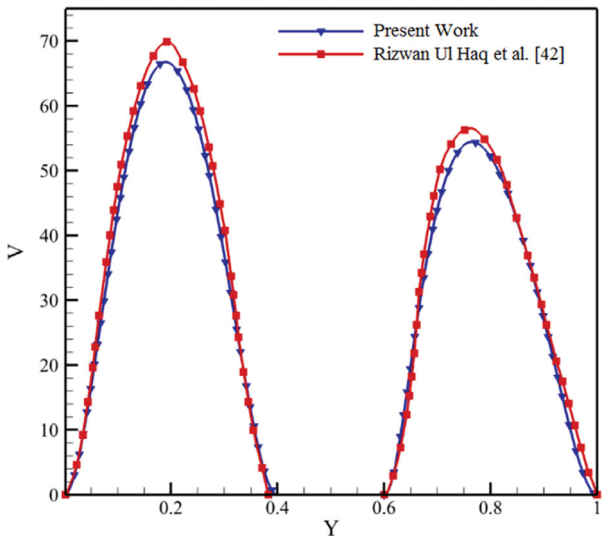

Fig. 3. The V-velocity along the Y-direction at (ϕ=0, Ra=10^5 and L_T = 0.4), obtained by present work and the results of Haq et al. [42].

ating the system regarding the variables. Afterward, the Galerkin matrix is formed by such equations. In the present work, grid refinement was performed using an adaptive technique, wherever the gradient of the variables is remarkable. The grid refinement proceeds until achieving the desired precision, which is defined by the user. To validate the numerical procedure, a comparison between the current simulation and the previous published paper by Haq et al. [42] was conducted, which is presented in Fig. 3. As shown, the v profile for $Ra=10^5$, $\phi=0$ and $L_T=0.4$ is plotted along the y-direction for both studies. It can be detected that an superb agreement with the (maximum) error of 5% is achieved, which demonstrating the accuracy of the model.

RESULTS AND DISCUSSION

The influences of the magnetic field and the radiation on the free convection in a partially heated hexagonal enclosed space filled with SWCNTs/water nanoliquid were explored numerically. In the current work, the Hartmann number is taken as $0\le Ha\le 100$, Rayleigh number varied as $10^4\le Ra\le 10^6$, heated region length varied as $0.1\le L_T\le 0.4$, various conditions of the internal hexagonal body (cold, adiabatic and heated), the solid-volume fraction varied as $0\le\phi\le 0.04$ and the radiation parameter varied as $0\le Rd\le 1$.

1. Effect of Rayleigh Number on the Flow, Thermal Fields, and Nusselt Number

The streamline (right) and isotherm (left) contours of the fluid for diverse values of Rayleigh numbers at $\phi=0.02$ and $L_T=0.2$ are graphically illustrated in Fig. 4. The stream field consists of two symmetrical revolving vortices around the internal hexagonal shaped body. These vortices are constructed as a result of the applied boundary conditions in the enclosed space. The hot light fluid adjacent the internal heated body begins to move upward until it reaches

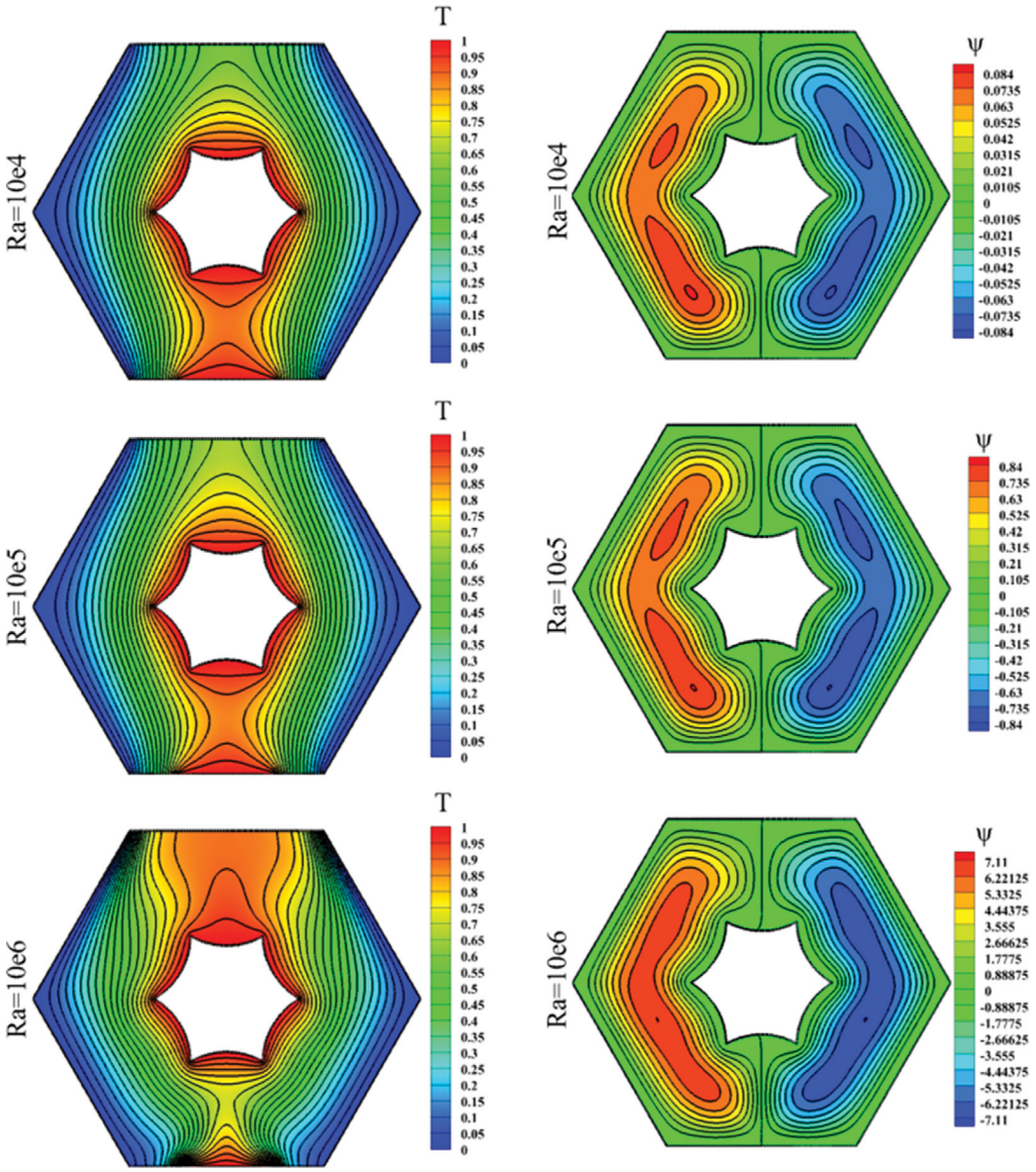

Fig. 4. Streamlines (right) and isotherms (left) for various Ra at ($\phi=0.02$, Ha=50 and Rd=0.5 and $L_T=0.2$).

the inclined cold walls of the enclosed space. After that, the fluid compresses and moves downward. The cyclic motion produces the two symmetrical rotating whirlpools inside the enclosed space. It is beneficial to remark that the intensity of the flow circulation can be evaluated by the Rayleigh number. At $Ra=10^4$, the magnitude of the stream function is very low also. The viscous force is predominant over the buoyancy one in this circumstance. Therefore, both effects of the buoyancy force and the free convection inside the enclosed space are slight. Now, when Rayleigh number rises from $Ra=10^4$ to $Ra=10^6$, a dramatic jump in stream function values can be seen. The maximum value rises from $\psi=0.084$ at $Ra=10^4$ to $\psi=7.11$ at $Ra=10^6$. The reason behind this severe rise is due to the high effect of the natural convection when Ra is high. Also, it can be noted from Fig. 4 that the flow field pattern changes its shape as Ra increases. The minor vortices which are seen when Ra is low begin to disappear at $Ra=10^6$. For the thermal field, when Ra is low $Ra=10^4$, the isotherm contours around the internal body are symmetrical, smooth, close to each other, uniform and parallel to the inclined walls of the enclosed space. Here, the heat is transported via conduction. Also, it can perceived from results of Fig. 4 that there is a high thermal gradient between the internal body and the partial heating area in the bottom wall, while the temperature begins to decline progressively as one goes towards the cold inclined walls. But, for $Ra=10^6$ the isotherm pattern begins to change significantly and elongates deeply especially at the upper space between the internal body and top wall of the enclosed space. Also, thermal plumes can be seen clearly in this space and an increase in the temperature can be noticed there. In this circumstance, the convection effects become dominant.

The variation of Nusselt numbers at the hexagonal enclosed space

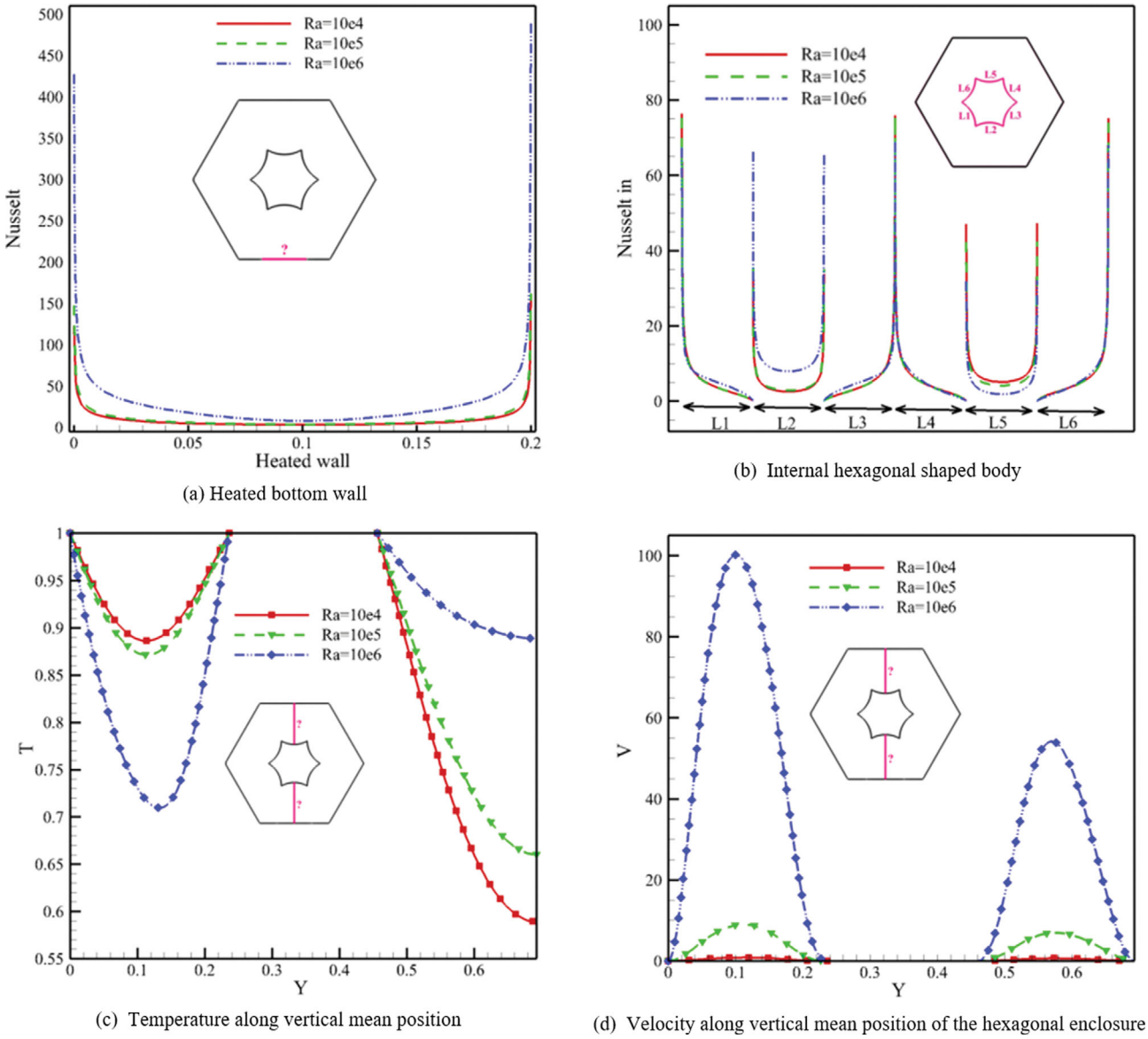

(a) Heated bottom wall

(b) Internal hexagonal shaped body

(c) Temperature along vertical mean position

(d) Velocity along vertical mean position of the hexagonal enclosure

Fig. 5. Variation of (a) Nusselt number, (b) Nusselt number at the internal shaped body, (c) temperature along vertically mean position, and (d) velocity along vertically mean position for various values of (Ra) at (ϕ=0.02, Ha=50, Rd=0.5 and L_T=0.2).

and internal hexagonal body, temperature and velocity for several values of Ra at ϕ=0.02 and L_T=0.2 are depicted, respectively, in Fig. 5(a)-(d). Fig. 5(a) shows that the Nusselt number along the heated bottom barrier of the hexagonal enclosed space Nu_{out} increases as Ra increases. This is due to the improvement in the free convection when Ra increases as a result of the dominant effect of the buoyancy force. Also, it can be noted that the Nusselt number begins to decline along the bottom heated wall until it reaches a certain value and then increases. This behavior can be detected for all measured values of Ra. The Nusselt number variation along different sides of the internal hexagonal body is illustrated in Fig. 5(b). For all values of Ra, the results show a symmetrical variation of Nusselt number at each considered side of the body (Nu_{in}). The maximum values of it can be seen for L_3 and L_4, while the minimum one can be found at L_5. Figs. 5(c) and (d) illustrate, respectively, the temperature and velocity distributions along vertical mean position of the hexagonal enclosed space for various values of Ra. For temperature, it can be seen that for vertical position below the internal body, it decreases with increase of Ra. While, a reverse behavior is noticed up the internal body. For velocity, it can be observed that it increases as (Ra) increases and its highest value corresponds to $Ra=10^6$. This behavior can be seen for all vertical positions up and below the internal hexagonal body.

2. Effect of Heated Region Length on the Flow, Thermal Fields, and Nusselt Number

Fig. 6 displays the streamline (right) and isotherm (left) contours

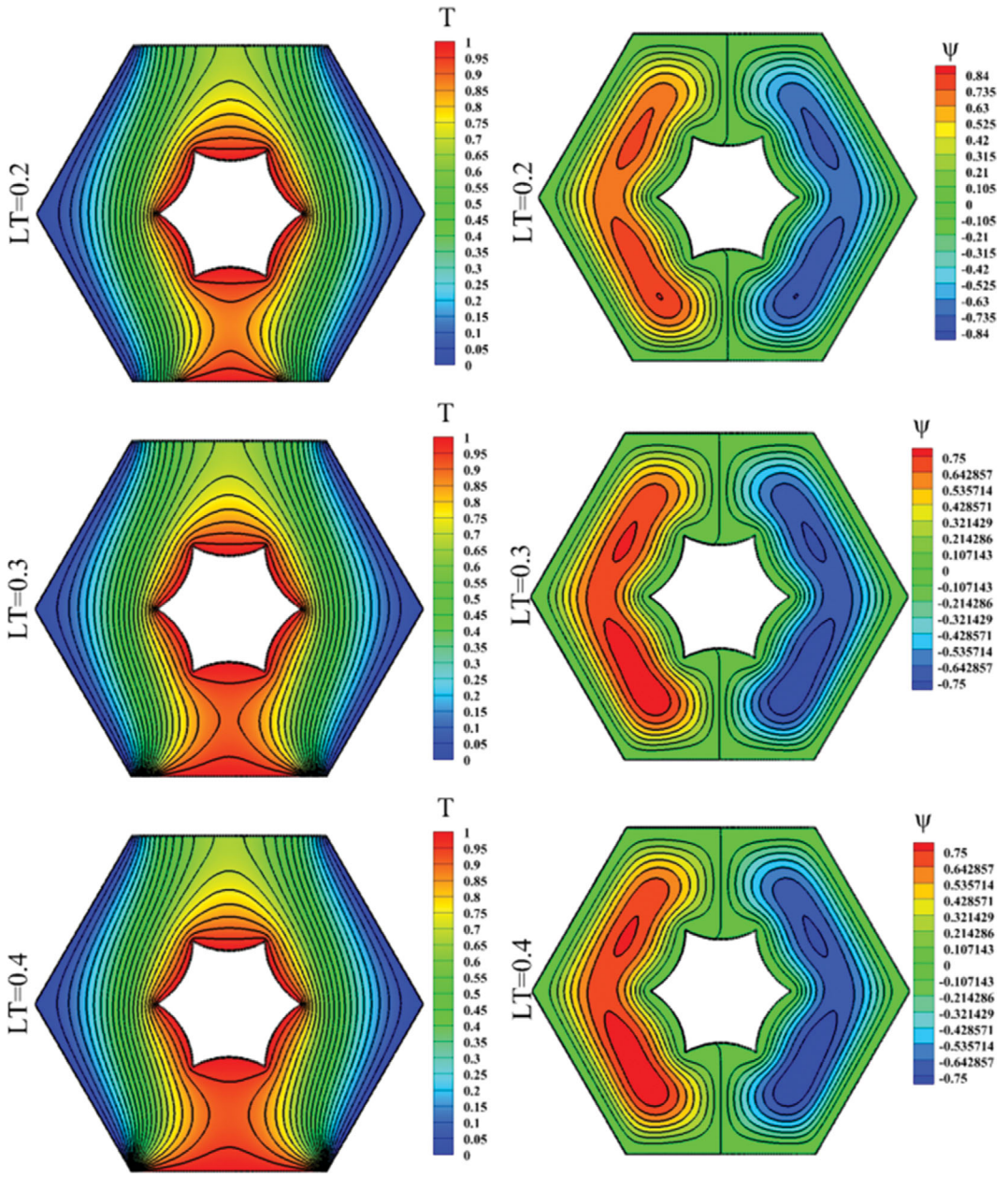

Fig. 6. Streamlines (right) and isotherms (left) for various values of heated region length in the bottom at (ϕ=0.02, Ha=50, Rd=0.5 and $Ra=10^5$).

of the nanoliquid for various values of heated region length in the bottom of the hexagonal enclosed space at ϕ=0.02 and Ra=10^5. It can be noticed that the stream circulation decreases as the heated region length increases. Its maximum value decreases from ψ=0.84 at L_T=0. To ψ=0.75 at L_T=0.4. Therefore, it can be deduced that the natural convection augments when the heated region length decreases. This is due to the decrease in the heat dissipation which produced by the shorter heated region length. This hints to raise the buoyancy force and enhance the strength of streamlines and the convection in the enclosed space. Also, the size of the upper core of vortices begins to reduce as the heated region length increases. For isotherms, it can be perceived that as the heated region length of the bottom wall increases, the isotherms begin to diverge from each other, especially in this region. This is due to the rise in the heat generation rate formed by the lengthier heated region and a high temperature gradient encountered in it. Therefore, the fluid temperature adjacent the heated region increases and makes the convection more dominant.

Fig. 7(a)-(c) explains the variation of Nusselt numbers at the hexagonal enclosed space and internal hexagonal body in addition to the temperature for several values of L_T at ϕ=0.02 and Ra=10^5. According to Fig. 7(a), the Nusselt number along the heated bottom wall of the hexagonal enclosed space, Nu_{out}, decreases as heated area size decreases. This means that the natural convection diminishes when the heated region span decreases. Moreover, Nu_{out} decreases along the heated wall until it attains a limited value and then increases after that. This behavior can be noted for all considered values of L_T. Fig. 7(b) depicts Nusselt number, Nu_{in}, along the length of the bottom side of the internal hexagonal body, L_2. For all values of L_T, a symmetrical behavior of Nusselt number pro-

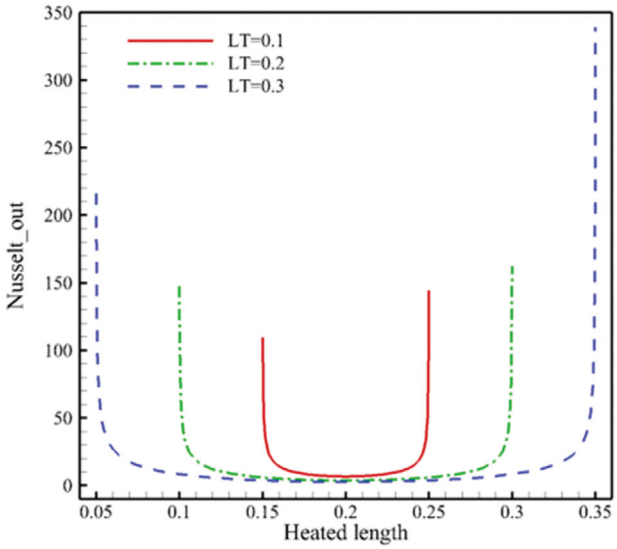

(a) Heated bottom wall

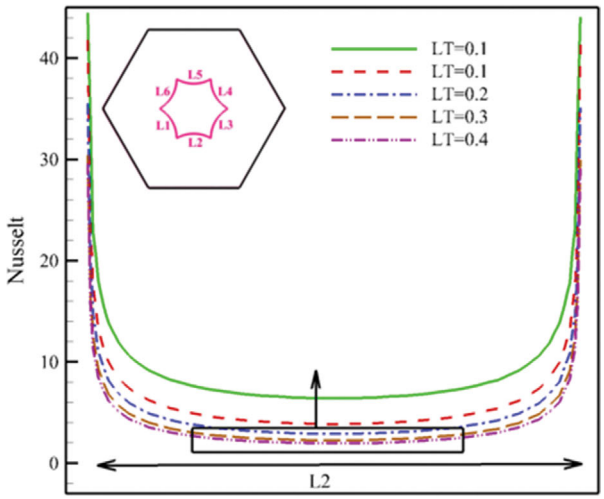

(b) Internal hexagonal shaped body

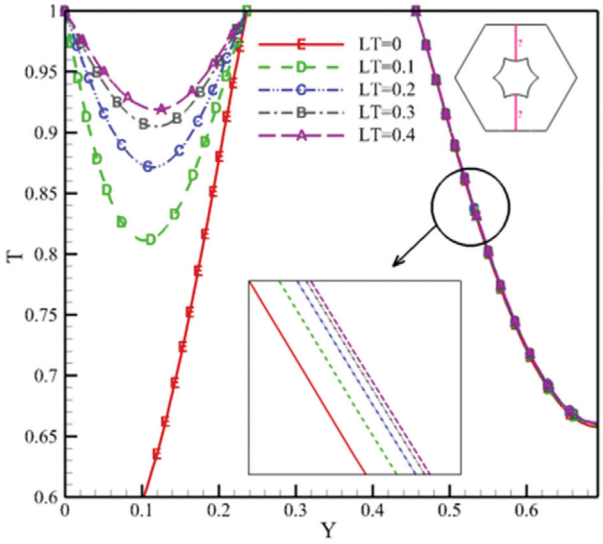

(c) Temperature along vertical mean position of the hexagonal enclosure

Fig. 7. Variation of (a) Nusselt number, (b) Nusselt number at the internal shaped body, and (c) temperature along vertical mean position for various values of (L_T) at (ϕ=0.02, Ha=50, Rd=0.5 and Ra=10^5).

files can be seen. It can be noted that value of Nu_{in} decreases as heated region length increases. Therefore, its maximum value corresponds to shorter heated region, L_T=0.1. This is due to the rise in the extreme temperature of the heated region by growing its length. This enhances the conduction effect and decreases the average Nusselt number. The temperature profiles along vertical mean position of the hexagonal enclosed space for various values of L_T are illustrated in Fig. 7(c). It is obvious that for vertical position below the internal body, it decreases with decrease of L_T. Whereas, the opposite behavior is noted up the internal body. Also, it can be noted that there is a clear variation in the temperature at the vertical position below the internal body. While, there is a very slight variation in it up this body.

3. Effect of Various Conditions of Internal Hexagonal Shaped Body on the Flow, Thermal Fields, and Nusselt Number

The streamline (right) and isotherm (left) contours for several conditions (adiabatic, cold, and heated) defined at the internal hexagonal body at ϕ=0.02, L_T=0.2 and Ra=10^5 are displayed in Fig. 8. It can be seen that the stream circulation of the nanoliquid increases as the conditions of the internal hexagonal body switch, respectively, from cold, adiabatic to heated boundary condition. Also, the pattern of the flow field is affected significantly according to these conditions. Therefore, for the cold condition, there are symmetrical rotating vortices which lie below the internal body and adjacent

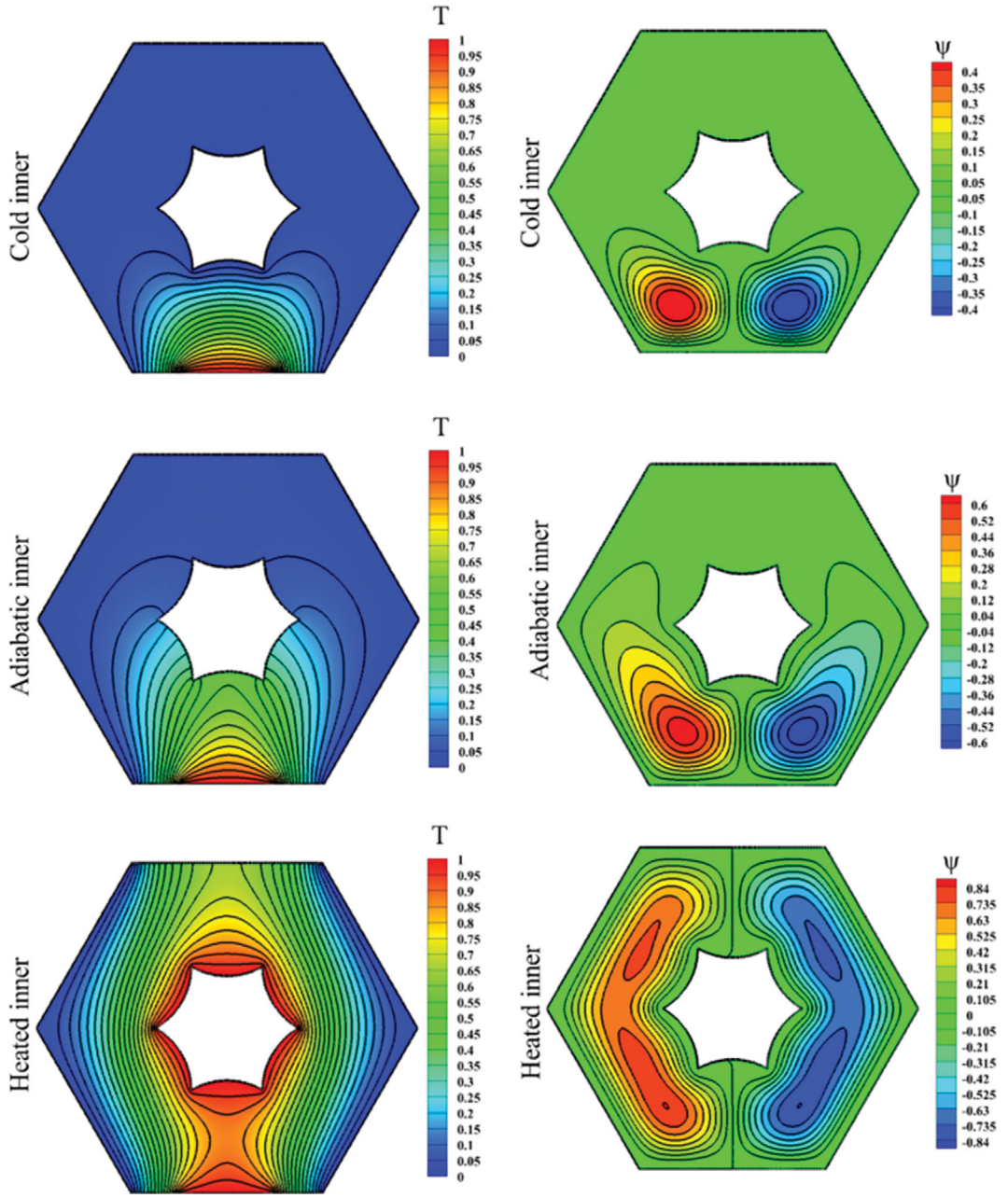

Fig. 8. Streamlines (right) and isotherms (left) for various conditions of internal hexagonal shaped body at (ϕ=0.02, L_T=0.2, Ha=50, Rd=0.5 and Ra=10^5).

the bottom wall of the hexagonal enclosed space. For adiabatic condition, the size of the vortices begins to increase clearly and expands further to reach the upper edge of the internal body. Now, for heated condition, the vortices size increases strongly and spreads in all region inside the hexagonal enclosed space. The maximum value of the stream function rises from ψ=0.4 for cold condition to ψ = 0.6 for adiabatic condition and ψ=0.84 for heated condition. Regarding isotherms, the thermal field is influenced also according to the circumstances of the internal body. For the cold condition, the isotherm lines are constructed near the heated region in the bottom wall and below the internal body. While, the regions inside the enclosed space remain cold. For the adiabatic condition, the isotherm lines spread further compared with the cold condition. They extend from the top of the adiabatic internal body to the heated region in the lowest wall of the hexagonal enclosed space. For the heated condition, the isotherms cover all the region of the hexagonal enclosed space. The hot nanoliquid spreads adjacent the heated area in the bottom wall and around the heated internal body. As one goes far from these regions, the temperature decreases gradually until it reaches the inclined cold walls.

The differences in Nusselt number at the hexagonal enclosed space, temperature and velocity for several conditions of the internal hexagonal body at ϕ=0.02, L_T=0.2 and Ra=10^5 are displayed in Fig. 9(a)-(c). As mentioned, three different types of the boundary conditions of this body were considered: cold, adiabatic and heated. Fig. 9(a) explains that the Nusselt number along the heated bottom wall of the hexagonal enclosed space (Nu_{out}) decreases as the conditions of the internal body switch respectively from cold, adiabatic to heated boundary condition. Again, the Nusselt number decreases along the bottom heated wall until it attains a limited value and then increases. This behavior is repeated for all considered conditions. For temperature, different profiles can be seen for

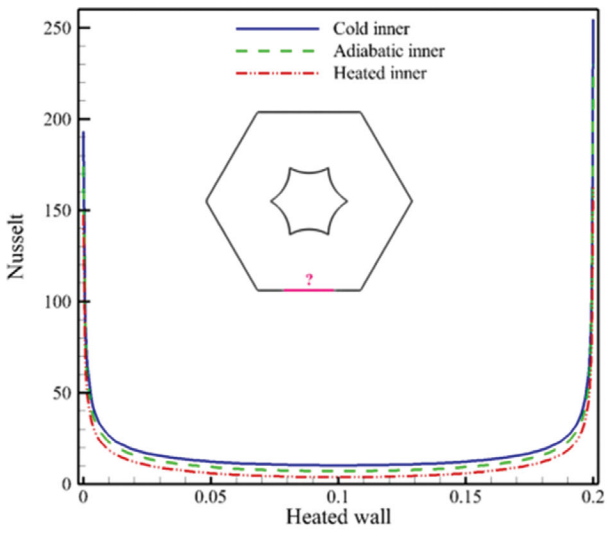

(a) Heated bottom wall

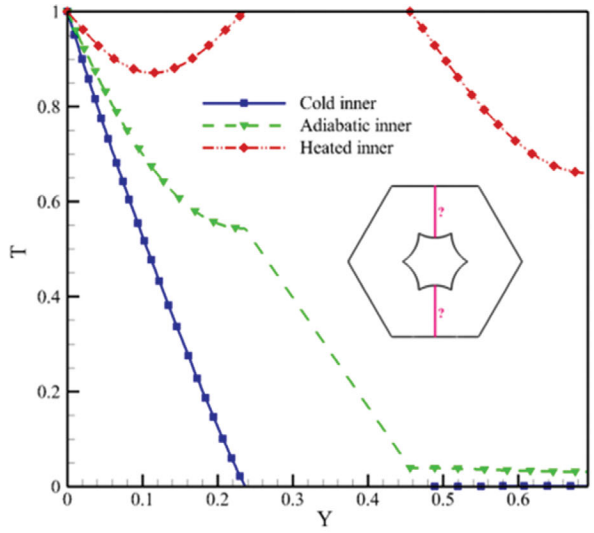

(b) Temperature along vertical mean position of the hexagonal enclosure

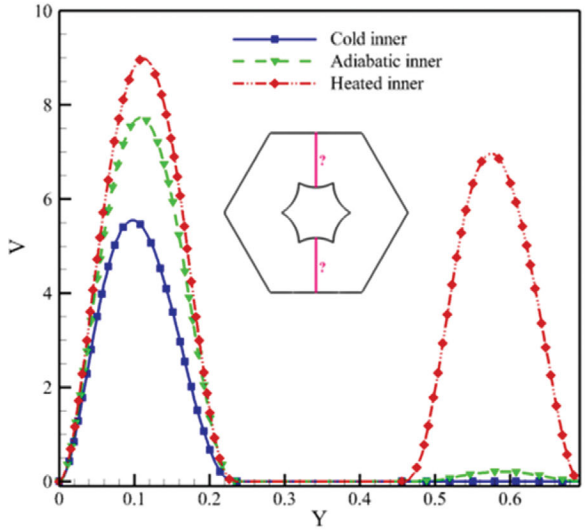

(c) Velocity along vertical mean position of the hexagonal enclosure

Fig. 9. Variation of (a) Nusselt number, (b) temperature along vertical mean position and (c) velocity along vertically mean position for various conditions of internal hexagonal shaped body at (ϕ=0.02, L_T=0.2, Ha=50, Rd=0.5 and Ra=10^5).

various considered conditions. As expected, the highest profile is found at the heated condition followed by the adiabatic one, while the cold condition has the lowest profile. For velocity, it can be seen also that the maximum profile is noted at the heated condition followed by the adiabatic one, while the cold condition has the minimum profile. This behavior is noted for all vertical positions up and below the internal hexagonal body.

4. Effect of Solid Volume Fraction on the Flow, Thermal Fields, and Nusselt Number

The streamline (right) and isotherm (left) contours for various values of solid volume fraction at L_T=0.2 and Ra=10^5 are graphically presented in Fig. 10. It can be seen that the value of the stream function decreases as the solid volume fraction rises. Its extreme value decreases from ψ=0.91 at ϕ=0 to ψ=0.77 at ϕ=0.04. Since the increase in ϕ leads to a high rise in the liquid viscosity and reduces the flow circulation. Therefore, the extreme stream circulation occurs for pure fluid (ϕ=0), whereas the minimum one occurs for nanoliquid (ϕ=0.04). Also, the cores of symmetrical vortices around the internal body begin to merge with each other as the solid volume fraction rises. For isotherms, the results of Fig. 10 indicate that the addition of nanoparticles to the water has a slight effect on their pattern. This can confirmed from the high similarity between them for all selected range of the solid volume fraction: 0≤ϕ≤0.04.

Fig. 11(a)-(d) shows profiles of Nusselt numbers at the hexagonal enclosed space and internal hexagonal body, temperature and velocity for various values of ϕ at L_T=0.2 and Ra=10^5. Fig. 11(a) displays that the Nusselt number along the heated bottom barrier

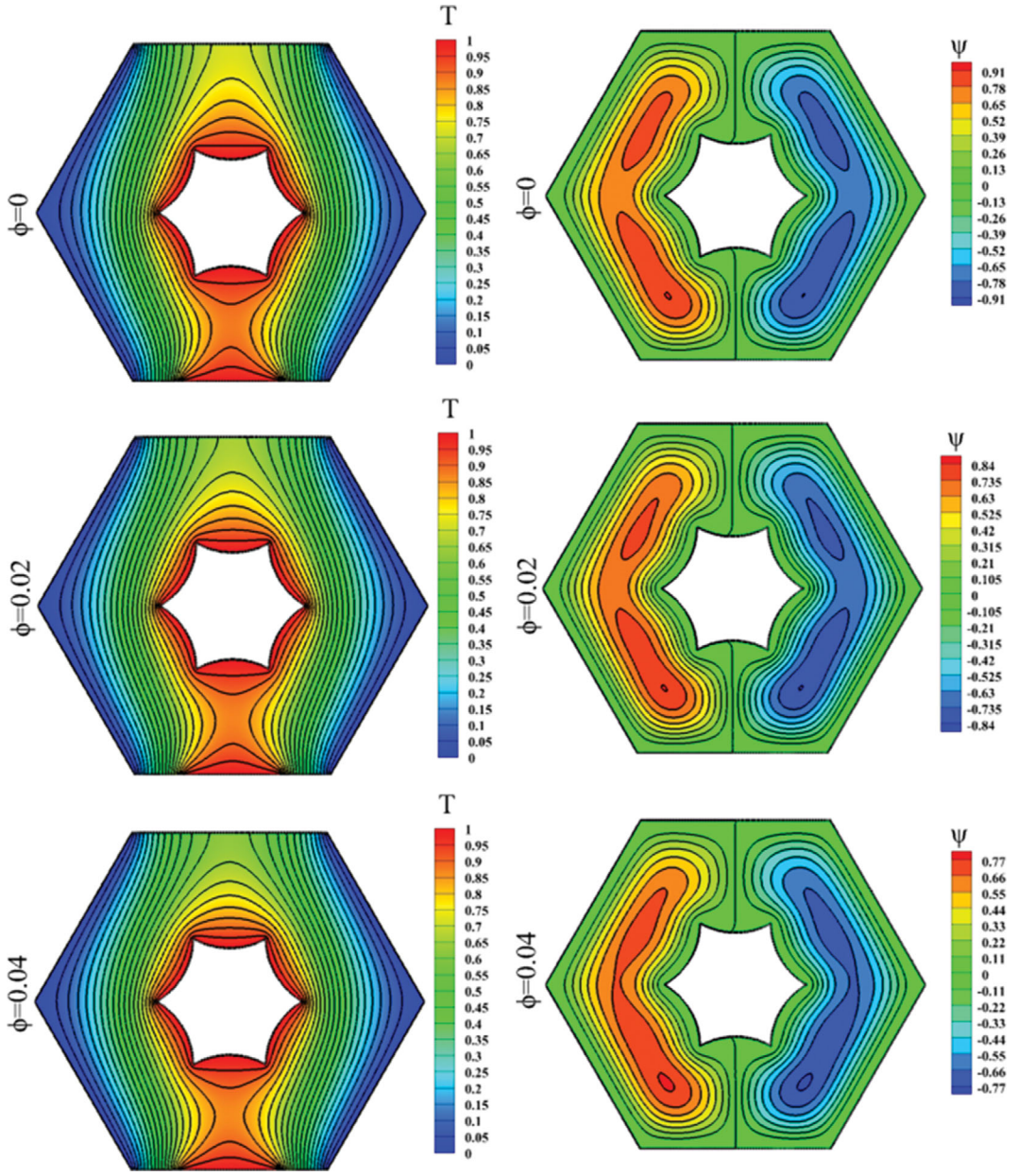

Fig. 10. Streamlines (right) and isotherms (left) for various values of solid volume fraction at (Rd=0.5, Ha=50, L_T=0.2 and Ra=10^5).

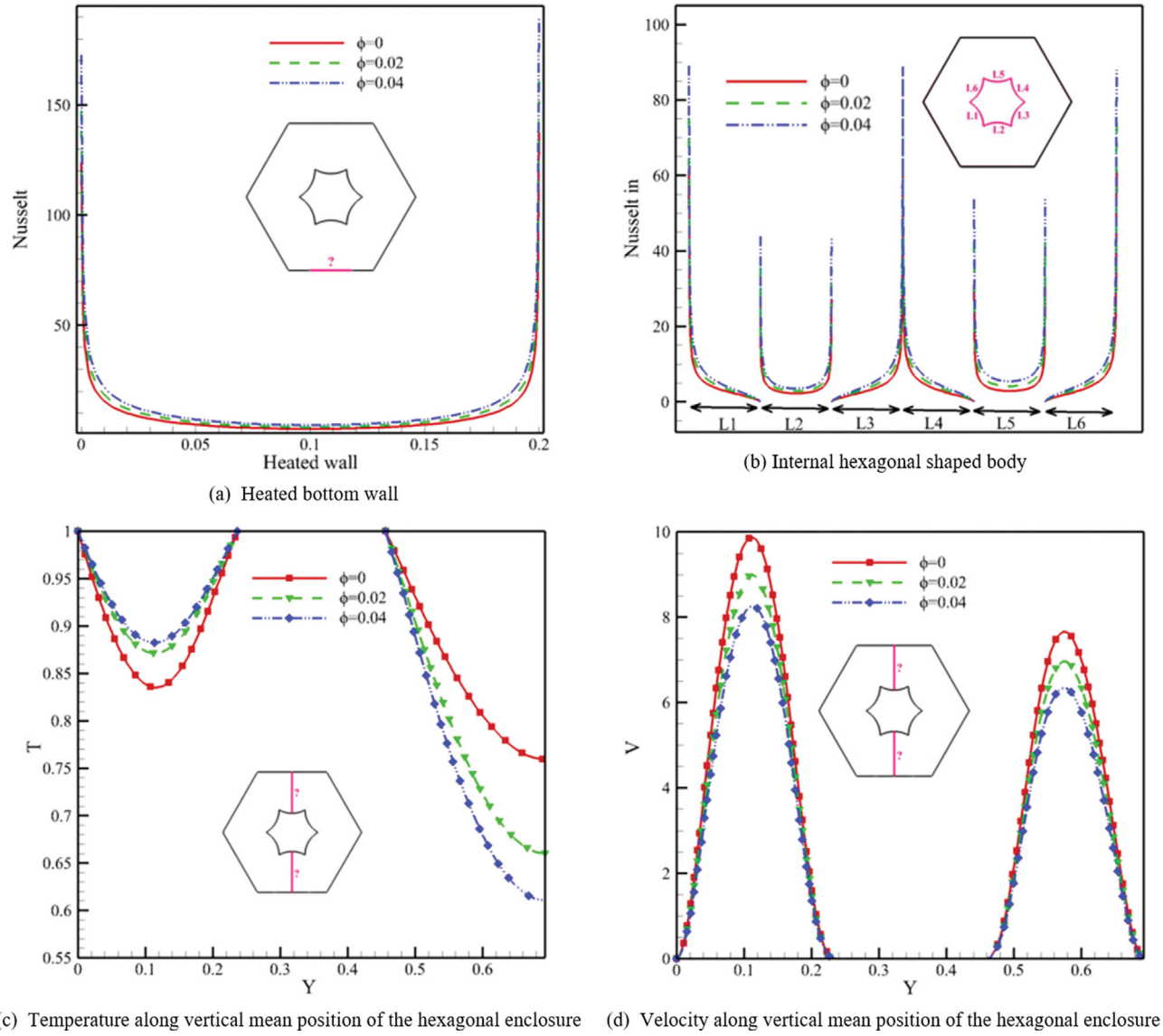

(a) Heated bottom wall

(b) Internal hexagonal shaped body

(c) Temperature along vertical mean position of the hexagonal enclosure

(d) Velocity along vertical mean position of the hexagonal enclosure

Fig. 11. Variation of (a) Nusselt number, (b) Nusselt number at the internal shaped body, (c) temperature along vertical mean position, and (d) velocity along vertical mean position for various values of (ϕ) at (Rd=0.5, Ha=50, L_T=0.2 and Ra=10^5).

of the hexagonal enclosed space, Nu_{out}, increases as the solid volume fraction increases. Since, the increase in ϕ enhances the heat transfer inside the enclosed space and accordingly the average Nusselt number increases. In addition, the Nusselt number begins to decline along the bottom heated wall until it reaches a limited value and increases after that. This observation is noted for all selected values of ϕ. Fig. 11(b) explains Nusselt number profiles (Nu_{in}) along different sides of the internal hexagonal body. Again, Nu_{in} increases as the solid volume fraction increases. Similar profiles are seen at each considered side of the body for all values of ϕ. The peak values of Nu_{in} can be observed for L_3 and L_4, whereas the lowest one can be seen at L_2. Figs. 11(c) and (d) depict, respectively, the temperature and velocity profiles along the vertical mean position of the hexagonal enclosed space for different values of ϕ. For temperature, it can be said that for vertical position below the internal body, it decreases with decrease of ϕ. Whereas, it increases with decrease of ϕ up this body. Also, the velocity decreases as ϕ increases and its peak value corresponds to ϕ=0. This result is noted for all vertical positions up and below the internal hexagonal body.

5. Effect of Hartmann Number on the Flow, Thermal Fields, and Nusselt Number

Fig. 12 illustrates streamline (right) and isotherm (left) contours in the hexagonal enclosed space for several values of Hartmann number at ϕ=0.02 , L_T=0.2 and Ra=10^5. It is beneficial to state that the relative significance of MHD flow can be measured via Hartmann number. When the magnetic field is absent (Ha=0), the strength of the flow circulation is high. Since, in this occasion, the free convection is significant due to the dominance of the buoyancy force. This offers to raise the stream function values. Now, when the magnetic field becomes predominant as the Hartmann number rises (50≤Ha≤100), the Lorentz force formed by the applied magnetic field becomes high and more effective. Whereas, the buoy-

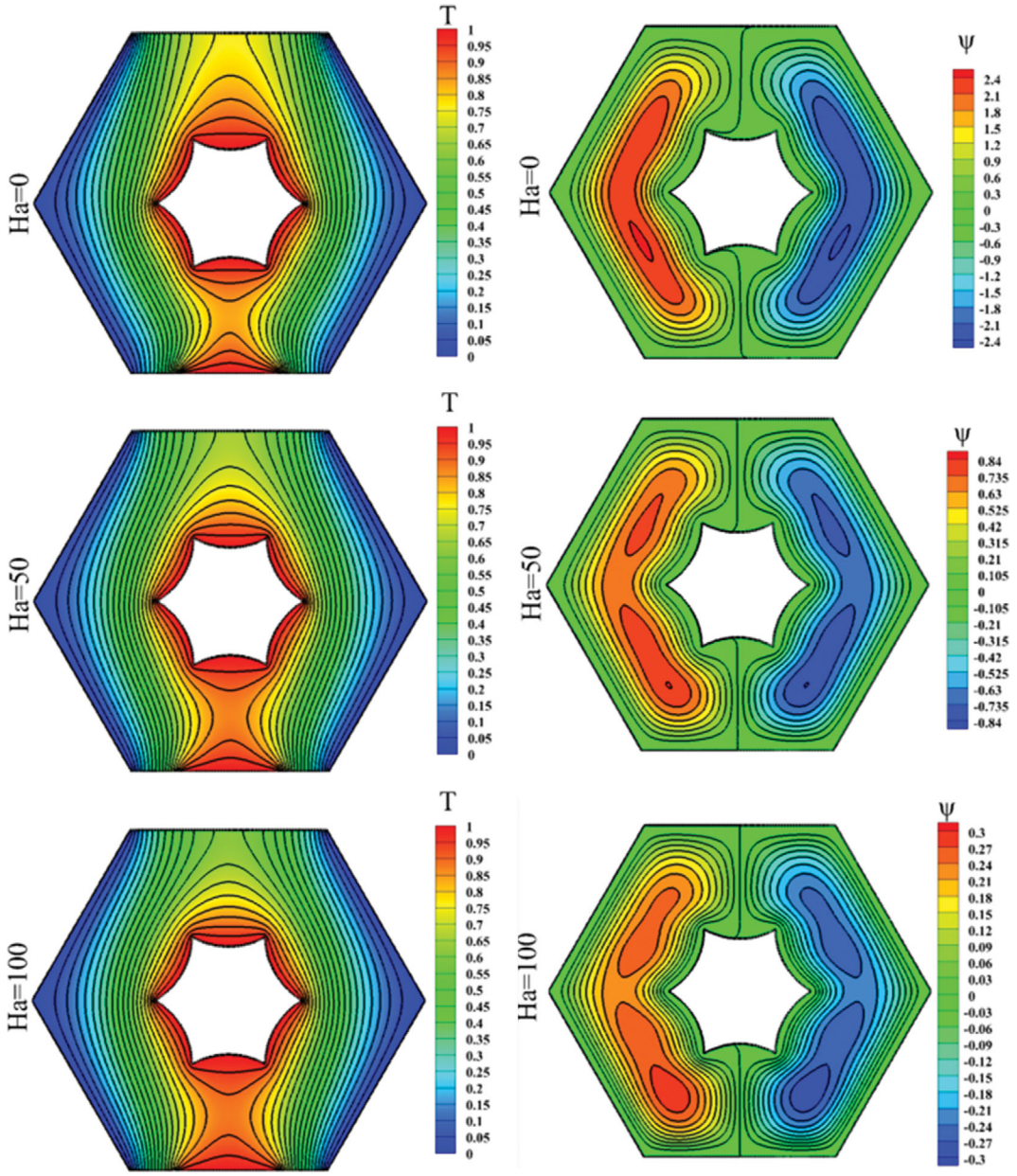

Fig. 12. Streamlines (right) and isotherms (left) for various values of Ha at (ϕ=0.02, L_T=0.2, Rd=0.5 and Ra=10^5).

ancy force begins to diminish gradually. This leads to a clear falling in the stream function value. It can be noted that, its maximum value decreases from ψ=2.4 at Ha=0 to ψ=0.3 at Ha=100. Therefore, it can be concluded that the magnetic field could be used efficiently to govern the natural convection inside the enclosed space. Also, it can be said that the increase in Ha affects the flow field pattern inside the enclosed space. Since, sizes of minor vortices begin to increase and convert from small single vortices at Ha=0 to multi-cellular vortices at Ha=100. For isotherms, it can be observed that for Ha=0 they are bunched intensely adjacent the heated bottom wall and around the internal body. In this case, their pattern is curved and close to each other, especially near the heated bottom wall and the convection is predominant. But, they begin to diverge from each other in the heated bottom wall and below the internal body as Hartmann number increases: 50≤Ha≤100. While, they converge clearly up the internal body compared with their corresponding isotherms at Ha=0. This observation indicates that the conduction is dominant at 50≤Ha≤100.

The distribution of Nusselt number at the hexagonal enclosed space, temperature and velocity for several values of Ha at ϕ=0.02, L_T=0.2 and Ra=10^5 are presented in Fig. 13(a)-(c). Fig. 13(a) refers that the Nusselt number, Nu_{out}, falls as Ha increases. This is because of the high influence of the magnetic field when the Ha increases. This weakens the natural convection, since the buoyancy force becomes smaller than the Lorentz force. So, the Nusselt number profile decreases and the minimum one corresponds to Ha=100. In the same manner, the Nusselt number decreases along the bottom heated wall until it attains a certain value and increases after

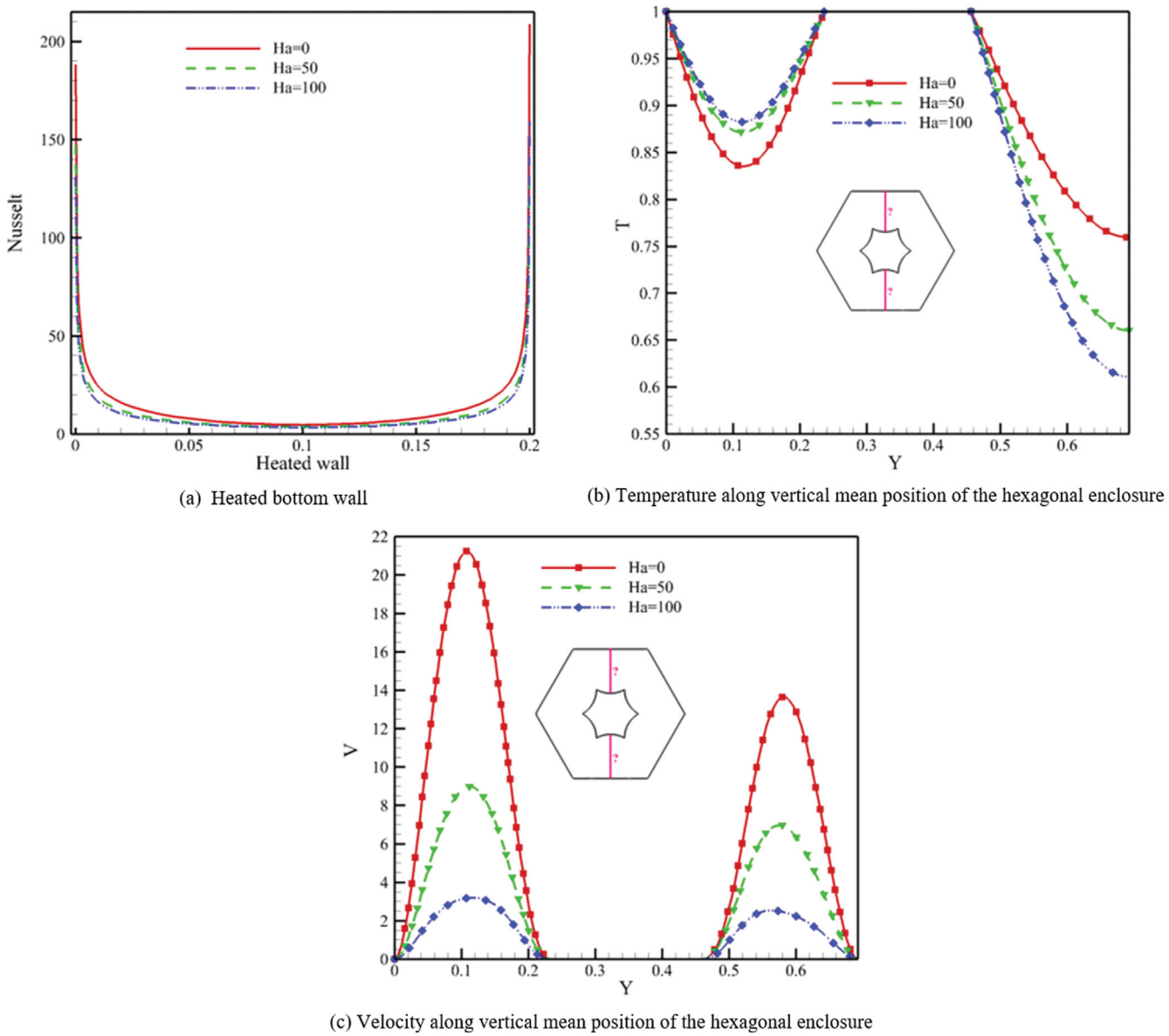

(a) Heated bottom wall

(b) Temperature along vertical mean position of the hexagonal enclosure

(c) Velocity along vertical mean position of the hexagonal enclosure

Fig. 13. Variation of (a) Nusselt number, (b) temperature along vertical mean position, and (c) velocity along vertically mean position for various values of (Ha) at (ϕ=0.02, L_T=0.2, Rd=0.5 and Ra=10^5).

it. The temperature and velocity curves along vertically mean position of the hexagonal enclosed space for various values of Ha are illustrated, respectively, in Figs. 13(b) and (c). For vertical position below the internal body, the temperature decreases as Ha decreases. While, it increases with decrease of Ha up this body. On the other hand, the velocity increases as Ha decreases and its minimum value matches to Ha=100. This notation is seen for all vertical positions up and below the internal hexagonal body.

6. Influence of Radiation Parameter on the Flow, Thermal Fields, and Nusselt Number

The streamline (right) and isotherm (left) contours inside the hexagonal enclosed space for various values of radiation parameter, Rd, at ϕ=0.02, L_T=0.2 and Ra=10^5 are demonstrated in Fig. 14. It is obvious from this graph that the increase in the radiation parameter from Rd=0 to Rd=1 has an effect on the rotating vortices pattern inside the enclosed space. The results of Fig. 14 indicate also that the size of rotating vortices amplifies as the radiation parameter increases. When the effect of the radiation is negligible, Rd=0, there are two symmetrical major vortices around the internal body. Now, at Rd=0.5 two minor vortices beside the previous major vortices are constructed below the internal body. While, the size of the minor vortices increases further at Rd=1. This is due to the heat transfer enhancement between the cold temperature of the inclined walls and the nanoliquid inside the enclosed space. Therefore, it can concluded that the radiation parameter has a positive role to improve the natural convection inside the enclosed space. For isotherms, it is seen that the rise in Rd clearly raises the temperature, especially in the spot between the heated bottom wall and below the internal body.

Fig. 15(a)-(d) explains, respectively, the variation of Nusselt num-

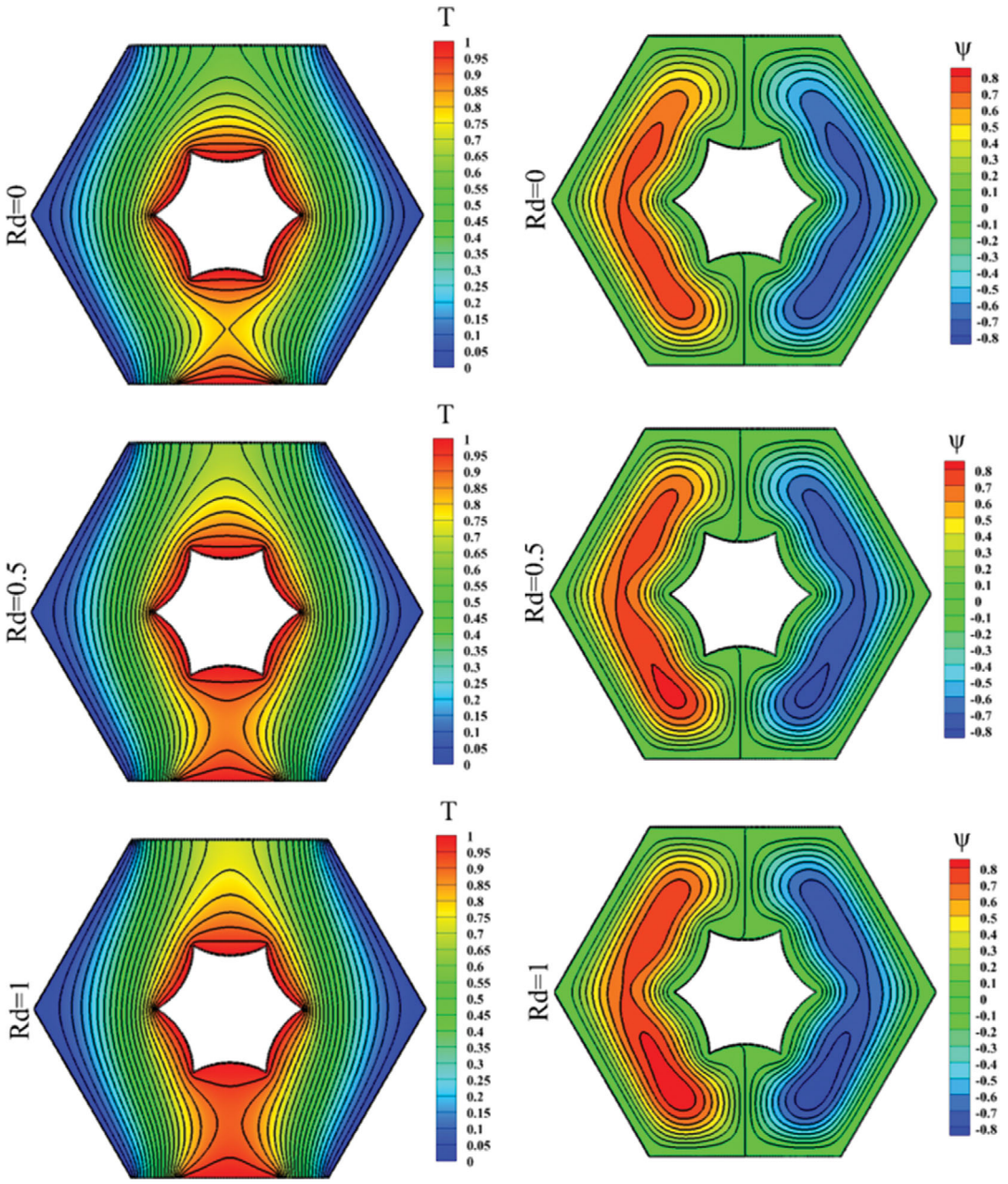

Fig. 14. Streamlines (right) and isotherms (left) for various values of Rd at (ϕ=0.02, L_T=0.2, Ha=50 and Ra=10^5).

bers at the hexagonal enclosed space and internal hexagonal body, temperature and velocity for various values of Rd at ϕ=0.02, L_T=0.2 and Ra=10^5. It can be perceived that Nu_{out} increases as the radiation parameter rises. This means that thermal radiation promotes the heat transmission between the enclosed space walls and the nanoliquid, leading to amplify the average Nusselt number. Moreover, the latter drops with the bottom heated wall until a limited value and increases after that. This notation is repeated for all measured values of Rd. The Nusselt number profiles (Nu_{in}) along various sides of the internal hexagonal body are displayed in Fig. 15(b). In a repeated manner, Nu_{in} arguments as the radiation parameter increases. The highest value of Nu_{in} corresponds to L and L_4, whereas the least value matches to L_2. For all values of Rd, symmetrical profiles are noted at each side of the body. The velocity and temperature profiles along vertical mean position of the hexagonal enclosed space for various values of Rd are presented in Figs. 15(c) and (d). For temperature, it can be observed that for vertical position below the internal body, it decreases with decrease of Rd. While, it increases with increase of Rd up this body. With respect to the velocity, it can be perceived that it rises as Rd rises for all vertical positions up and below the internal body.

CONCLUSIONS

The natural convection and flow field of SWCNTs/water nanoliquid inside a partially heated hexagonal enclosed space was stud-

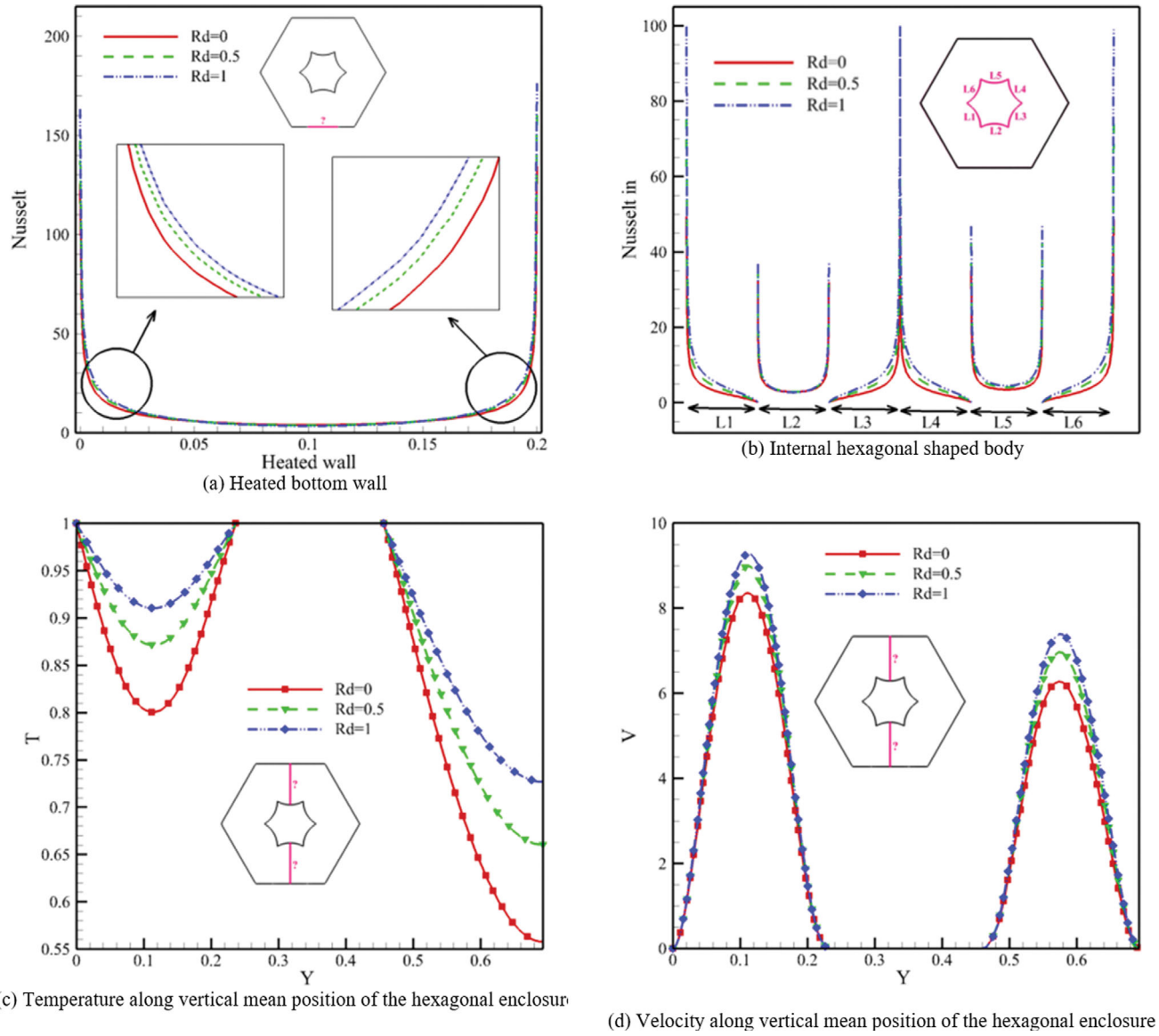

(a) Heated bottom wall

(b) Internal hexagonal shaped body

(c) Temperature along vertical mean position of the hexagonal enclosur

(d) Velocity along vertical mean position of the hexagonal enclosure

Fig. 15. Variation of (a) Nusselt number, (b) Nusselt number at the internal shaped body, (c) temperature along vertically mean position, and (d) velocity along vertical mean position for various values of (Rd) at (ϕ=0.02, L_T=0.2, Ha=50 and Ra=10^5).

ied. The impact of thermal radiation and magnetic field on stream and heat transfer was investigated. Similarity variables were defined for non-dimensionalizing the governing equations and the SGFEM is used for solving the final series of equations. The following conclusions can be observed from the outcomes of the current work:

- Both Nu_{out} and velocity distribution along vertically mean position rise as Ra rises.
- For all values of Ra, the extreme values of Nu_{in} can be seen for L_3 and L_4, while the minimum one can be found at L_5.
- When L_T decreases, Nu_{out} decreases. While, values of (Nu_{in}) decrease as it increases.
- Temperature at the vertical position below the internal body decreases with decrease of (L_T) and increase of Ra. Whereas, an opposite behavior is noted up this body.
- Both Nu_{out} and Nu_{in} increase as ϕ and Rd increase. While, the stream function and Nu_{out} fall as Ha increases.
- Velocity decreases as ϕ increases and its peak value is at ϕ=0. While, it increases as Rd increases and Ha decreases for all vertical positions up and below the internal body.
- The temperature at the vertical position below the internal body decreases with decrease of Rd, ϕ and Ha. While, it augments with increase ofRd and decrease of both Ha and ϕ up this body.

ACKNOWLEDGEMENTS

The third author (Ahmed Kadhim Hussein) would like to express his deepest gratitude to Mrs. Topsy N. Smalley from the United States of America for her kind assistance.

REFERENCES

1. K. Ghachem, L. Kolsi, C. Mâatki, A. K. Hussein and M. Borjini, *Int.*

Commun. Heat Mass Transf., **39**, 869 (2012).
2. A. S. Alshomrani, S. Sivasankaran, A. A. Amer and A. Biswas, *Numer. Heat Transf.; A: Appl.*, **76**, 87 (2019).
3. M. Elkhazen, W. Hassen, R. Gannoun, A. K. Hussein and M. Borjini, *J. Eng. Phys. Thermophys.*, **92**, 1318 (2019).
4. S. Hussain and A. K. Hussein, *Int. Commun. Heat Mass Transf.*, **37**, 1115 (2010).
5. A. M. Rashad, S. Sivasankaran, M. A. Mansour and M. Bhuvaneswari, *Numer. Heat Transf.; A: Appl.*, **71**, 1223 (2017).
6. S. Sivasankaran, M. A. Mansour, A. M. Rashad and M. Bhuvaneswari, *Numer. Heat Transf. A*, **70**, 1356 (2016).
7. S. Ahmed, A. K. Hussein, M. Abd El-Aziz and S. Sivasankaran, *Heat Transf. Res.*, **47**, 383 (2016).
8. S. Sivasankaran, H. T. Cheong, M. Bhuvaneswari and P. Ganesan, *Numer. Heat Transf. A*, **69**, 630 (2016).
9. R. Bindhu, G. Sai SundaraKrishnan, S. Sivasankaran and M. Bhuvaneswari, *Energy Environ.*, **30**, 833 (2019).
10. S. Ahmed, A. K. Hussein, H. Mohammed, I. Adegun, X. Zhang, L. Kolsi, A. Hasanpour and S. Sivasankaran, *Nucl. Eng. Des.*, **266**, 34 (2014).
11. A. K. Hussein, H. Ashorynejad, S. Sivasankaran, L. Kolsi, M. Shikholeslami and I. Adegun, *Alex. Eng. J.*, **55**, 203 (2016).
12. S. Sivasankaran and K. Narrein, *IJST-T Mech Eng.*, **44**, 373 (2020).
13. R. Chand, G. Rana and A. K. Hussein, *J. Appl. Fluid Mech.*, **8**, 265 (2015).
14. R. Mashayekhi, E. Khodabandeh, O. Akbari, D. Toghraie, M. Bahiraei and M. Gholami, *J. Therm. Anal. Calorim.*, **134**, 2305 (2018).
15. M. Bayat, M. Faridzadeh and D. Toghraie, *Therm. Sci. Eng. Prog.*, **5**, 50 (2018).
16. A. Kareem, H. Mohammed, A. K. Hussein and S. Gao, *Int. Commun. Heat Mass Transf.*, **77**, 195 (2016).
17. A. Al-Rashed, K. Kalidasan, L. Kolsi, R. Velkennedy, A. Aydi, A. K. Hussein and E. Malekshah, *Int. J. Mech. Sci.*, **135**, 362 (2018).
18. M. Esfe, M. Akbari, D. Toghraie, A. Karimipour and M. Afrand, *Heat Transf. Res.*, **45**, 409 (2014).
19. H. Bazdar, D. Toghraie, F. Pourfattah, O. Akbari, H. Nguyen and A. Asadi, *J. Therm. Anal. Calorim.*, **139**, 2365 (2020).
20. H. Arasteh, R. Mashayekhi, M. Goodarzi, S. Motaharpour, M. Dahari and D. Toghraie, *J. Therm. Anal. Calorim.*, **138**, 1461 (2019).
21. B. Ruhani, P. Barnoon and D. Toghraie, *Phys. A*, **525**, 616 (2019).
22. M. Kamel, F. Lezsovits and A. K. Hussein, *J. Therm. Anal. Calorim.*, **138**, 4019 (2019).
23. M. Ali, M. Alim and S. Ahmed, *Procedia Eng.*, **194**, 479 (2017).
24. R. Vignesh Kumar and P. Devan, Proceedings of IHMTC2019-HTE-779 (2019).
25. L. Kolsi, A. K. Hussein, M. Borjini, H. Mohammed and H. Ben Aïssia, *Arab J. Sci. Eng.*, **39**, 7483 (2014).
26. S. Hussain and A. K. Hussein, *J. Heat Trans. - T ASME*, **136**, 082502 (2014).
27. A. K. Hussein and S. Hussain, *Alex. Eng. J.*, **55**, 169 (2016).
28. A. K. Hussein and A. Mustafa, *Therm. Sci. Eng. Prog.*, **1**, 66 (2017).
29. A. K. Hussein and A. Mustafa, *Heat Transf. - Asian Res.*, **47**, 320 (2018).
30. E. Sourtiji and S. Hosseinizadeh, *Therm. Sci.*, **16**, 489 (2012).
31. M. Sheikholeslami, M. Gorji-Bandpy and D. Ganji, *Energy*, **60**, 501 (2013).
32. M. Sheikholeslami, D. Ganji, M. Gorji-Bandpy and S. Soleimani, *J. Taiwan Inst. Chem. Eng.*, **45**, 795 (2014).
33. A. Al-Zamily, *Comput. Fluids*, **103**, 71 (2014).
34. H. Elshehabey, F. Hady, S. Ahmed and R. Mohamed, *Int. Commun. Heat Mass Transf.*, **57**, 228 (2014).
35. A. K. Hussein, M. Bakier, M. Ben Hamida and S. Sivasankaran, *Alex. Eng. J.*, **55**, 2157 (2016).
36. M. Ali, M. Alim, R. Akhter and S. Ahmed, *Int. J. Appl. Comput. Math.*, **3**, 1047 (2017).
37. A. Yadollahi, A. Khalesidoost, A. Kasaeipoor, M. Hatami and D. Jing, *Eur. Phys. J. Plus*, **132**, 372 (2017).
38. A. Dogonchi, F. Selimefendigil and D. D. Ganji, *Int. J. Numer. Method Heat Fluid Flow*, **29**, 1663 (2019).
39. A. Purusothaman and E. Malekshah, *Therm. Sci. Eng. Prog.*, **10**, 186 (2019).
40. S. M. Seyyedi, A. S. Dogonchi, M. Hashemi-Tilehnoee, D. D. Ganji and A. J. Chamkha, *Int. J. Numer. Method Heat Fluid Flow*, **30**(11), 4811 (2020).
41. M. Sheikholeslami, M. Gorji-Bandpy, D. D. Ganji and S. Soleimani, *Adv. Powder Technol.*, **24**, 980 (2013).
42. R. Ul-Haq and S. Aman, *Int. J. Heat Mass Transf.*, **128**, 401 (2019).
43. M. Sheikholeslami, M. Gorji-Bandpy and K. Vajravelu, *Int. J. Heat Mass Transf.*, **80**, 16 (2015).
44. A. K. Hussein, H. Ashorynejad, M. Sheikholeslami and S. Sivasankaran, *Nucl. Eng. Des.*, **268**, 10 (2014).
45. K. Narrein, S. Sivasankaran and P. Ganesan, *Numer. Heat Transf. A*, **69**, 921 (2016).
46. Z. Li, A. K. Hussein, O. Younis, S. Rostami and W. He, *Int. Commun. Heat Mass Transf.*, **112**, 104497 (2020).
47. M. Sheremet, I. Pop and A. Rosca, *Int. J. Numer. Method Heat Fluid Flow*, **28**, 1738 (2018).
48. A. Mostafazadeh, D. Toghraie, R. Mashayekhi and O. Akbari, *J. Therm. Anal. Calorim.*, **138**, 779 (2019).
49. M. Sheikholeslami, D. D. Ganji and M. Rashidi, *J. Taiwan Inst. Chem. Eng.*, **47**, 6 (2015).
50. Z. Li, A. K. Hussein, O. Younis, M. Afrand and S. Feng, *Int. Commun. Heat Mass Transf.*, **116**, 104650 (2020).
51. S. Yan, M. Fazilati, N. Samani, H. Ghasemi, D. Toghraie, Q. Nguyen and A. Karimipour, *J. Energy Storage*, **30**, 101445 (2020).
52. A. Moraveji and D. Toghraie, *Int. J. Heat Mass Transf.*, **113**, 432 (2017).